interaction data from two evolutionarily distant species. Our data strongly support the idea that functional modules are highly conserved, but the wiring between them can differ substantially. Thus, the use of model systems to make inferences about biological network topology may be more successful for describing modules than for describing the cross talk between them.

References and Notes

1. M. Schuldiner *et al.*, *Cell* **123**, 507 (2005).
2. S. R. Collins *et al.*, *Nature* **446**, 806 (2007).
3. X. Pan *et al.*, *Methods* **41**, 206 (2007).
4. A. H. Y. Tong *et al.*, *Science* **303**, 808 (2004).
5. A. Roguev, M. Wiren, J. S. Weissman, N. J. Krogan, *Nat. Methods* **4**, 861 (2007).
6. J. Tischler, B. Lehner, A. G. Fraser, *Nat. Genet.* **40**, 390 (2008).
7. Materials and methods are available as supporting material on *Science* Online.
8. S. R. Collins, M. Schuldiner, N. J. Krogan, J. S. Weissman, *Genome Biol.* **7**, R63 (2006).
9. C. Stark *et al.*, *Nucleic Acids Res.* **34**, D535 (2006).
10. R. Kaur, C. F. Kostrub, T. Enoch, *Mol. Biol. Cell* **12**, 3744 (2001).
11. J. Majka, P. M. Burgers, *Proc. Natl. Acad. Sci. U.S.A.* **100**, 2249 (2003).
12. A. Ghavidel *et al.*, *Cell* **131**, 915 (2007).
13. N. J. Krogan *et al.*, *Mol. Cell* **12**, 1565 (2003).
14. G. Mizuguchi *et al.*, *Science* **303**, 343 (2004), published 26 November 2003; 10.1126/science.1090701.
15. M. S. Kobor *et al.*, *PLoS Biol.* **2**, E131 (2004).
16. S. Ahmed, B. Dul, X. Qiu, N. C. Walworth, *Genetics* **177**, 1487 (2007).
17. A. Roguev *et al.*, *EMBO J.* **20**, 7137 (2001).
18. N. J. Krogan *et al.*, *J. Biol. Chem.* **277**, 10753 (2002).
19. A. Roguev *et al.*, *J. Biol. Chem.* **278**, 8487 (2003).
20. P. L. Nagy, J. Griesenbeck, R. D. Kornberg, M. L. Cleary, *Proc. Natl. Acad. Sci. U.S.A.* **99**, 90 (2002).
21. A. C. Gavin *et al.*, *Nature* **415**, 141 (2002).
22. A. Roguev *et al.*, *Mol. Cell. Proteomics* **3**, 125 (2004).
23. B. Dichtl *et al.*, *Mol. Cell* **10**, 1139 (2002).
24. S. I. Grewal, S. Jia, *Nat. Rev. Genet.* **8**, 35 (2007).
25. M. Zofall, S. I. Grewal, *Mol. Cell* **22**, 681 (2006).
26. T. Sugiyama *et al.*, *Cell* **128**, 491 (2007).
27. K. R. Hansen *et al.*, *Mol. Cell. Biol.* **25**, 590 (2005).
28. H. P. Cam, K. Noma, H. Ebina, H. L. Levin, S. I. Grewal, *Nature* **451**, 431 (2008).
29. N. J. Krogan *et al.*, *Nature* **440**, 637 (2006).
30. H. Spahr *et al.*, *J. Biol. Chem.* **275**, 1351 (2000).
31. H. Sakurai, M. Kimura, A. Ishihama, *Gene* **221**, 11 (1998).
32. D. N. Millband, K. G. Hardwick, *Mol. Cell. Biol.* **22**, 2728 (2002).
33. X. Liu, I. McLeod, S. Anderson, J. R. Yates III, X. He, *EMBO J.* **24**, 2919 (2005).
34. K. Asakawa *et al.*, *Mol. Biol. Cell* **17**, 1421 (2006).
35. I. M. Hall, K. Noma, S. I. Grewal, *Proc. Natl. Acad. Sci. U.S.A.* **100**, 193 (2003).
36. G. Otero *et al.*, *Mol. Cell* **3**, 109 (1999).
37. J. Gardiner, D. Barton, J. Marc, R. Overall, *Traffic* **8**, 1145 (2007).
38. M. Sipiczki, *Genome Biol.* **1**, REVIEWS1011 (2000).
39. C. J. Penkett, J. A. Morris, V. Wood, J. Bahler, *Nucleic Acids Res.* **34**, W330 (2006).
40. B. E. Dul, N. C. Walworth, *J. Biol. Chem.* **282**, 18397 (2007).
41. S. Bandyopadhyay, R. Kelley, N. J. Krogan, T. Ideker, *PLOS Comput. Biol.* **4**, e1000065 (2008).

42. We thank P. Beltrao and G. Cagney for critical reading of the manuscript; M. Wiren and S. Forsburg for discussion; P. Kemmeren for setting up the web database; S. Wang, C. Wen, and D. Avdic for technical help; and F. Stewart for sharing unpublished data. This work was supported by NIH [National Institute of General Medical Sciences grant GM084279 (T.I. and N. J.K.)], the Sandler Family Foundation (N.J.K), the Howard Hughes Medical Institute (J.S.W.), National Cancer Institute (S.I.G.), Center for Cancer Research (S.I.G.), and the California Institute of Quantitative Biology (N.J.K.).

Supporting Online Material

www.sciencemag.org/cgi/content/full/1162609/DC1
Materials and Methods
SOM Text
Figs. S1 to S5
Tables S1 to S8
References
Databases S1 to S4

1 July 2008; accepted 12 September 2008
Published online 25 September 2008;
10.1126/science.1162609
Include this information when citing this paper.

REPORTS

Current-Induced Spin-Wave Doppler Shift

Vincent Vlaminck and Matthieu Bailleul

Spin transfer appears to be a promising tool for improving spintronics devices. Experiments that quantitatively access the magnitude of the spin transfer are required for a fundamental understanding of this phenomenon. By inductively measuring spin waves propagating along a permalloy strip subjected to a large electrical current, we observed a current-induced spin wave Doppler shift that we relate to the adiabatic spin transfer torque. Because spin waves provide a well-defined system for performing spin transfer, we anticipate that they could be used as an accurate probe of spin-polarized transport in various itinerant ferromagnets.

Spin transfer—the transfer of angular momentum produced by a flow of electrons through an inhomogeneous magnetization configuration (*1*, *2*)—has many potential applications for data storage and microwave electronics. It has been demonstrated recently in nanostructured multilayers [current-induced magnetic switching (*3*, *4*) and precession (*5*, *6*)] and extended magnetic strips [current-induced domain-wall motion (*7*, *8*)]. It is usually difficult to measure the magnitude of the spin transfer with such experiments because they involve a complex spatiotemporal evolution of the magnetization (*4*, *8*). As recently suggested, spin transfer can also occur when an electrical current flows through a spin wave (*9*, *10*), which has the advantage of being a system that is stationary both in time and space: The low-amplitude magnetization perturbation is entirely determined by the wave vector $\vec{k}$ and pulsation ω of the spin wave (Fig. 1A), and the standard adiabatic gradient expression of spin transfer torque (STT) for continuously variable magnetization (*11*–*14*) results in a simple shift of the frequency of the spin wave (*10*, *15*)

$$\Delta\omega_{\mathrm{STT}} = \frac{P\mu_{\mathrm{B}}}{-|e|M_{\mathrm{s}}}\vec{J}\vec{k} \qquad (1)$$

where P is the degree of spin polarization of the electrical current, μ_{B} is the Bohr magneton, $\vec{J}$ is the electrical current density, e is the electron charge, and M_{s} is the saturation magnetization. Although this current-induced frequency shift should not be confused with a true Doppler shift (*16*) that occurs, for example, when a detector is moved along the ferromagnet in which the spin wave propagates (*17*), it can be identified formally as the Doppler shift that would occur if the full electron system were simply drifting with respect to the lab frame with a velocity of $P\mu_{\mathrm{B}}\vec{J}/-|e|M_{\mathrm{s}}$, as suggested 40 years ago by Lederer and Mills (*18*).

We used a micrometer-sized version of the propagating spin wave spectroscopy (PSWS) technique (*19*–*21*). The microfabricated sample (Fig. 1, B and C) consisted of a permalloy ($Ni_{80}Fe_{20}$) strip [width (w) = 2 μm, thickness (t) = 20 nm], at the extremities of which four metal pads served to inject the current I_{dc} and measure the resistance. An external field H_0 ($\mu_0 H_0 \sim 1$ T, where μ_0 is the permeability of the vacuum) magnetized the permalloy strip out of plane so that spin waves propagated in the so-called magnetostatic forward volume waves (MSFVW) geometry (*19*, *20*). Spin waves were emitted and detected with a pair of spin wave antennae (center-to-center distance D = 7.7 μm) located above the central part of the strip and connected to a 20-GHz vector network analyzer via coplanar waveguides (CPW). Each antenna consists of a sub-micrometer–sized meander terminated with a short circuit. In the operating principle of PSWS (Fig. 1E), a microwave current $i(\omega)$ is injected into one antenna and generates a microwave magnetic field $h(\omega)$ that couples to the spin wave modes $m(\omega,k)$. These spin waves propa-

Institut de Physique et Chimie des Matériaux de Strasbourg, UMR 7504 CNRS–Université Louis Pasteur, 23 Rue du Loess, 67034 Strasbourg Cedex 2, France.

gate in both directions along the strip and induce an additional magnetic flux on the excitation antenna and on the second antenna. The signature of the spin waves is therefore a magnetic resonance behavior for the self-inductance $\Delta L_{11}(\omega)$ of the excitation antenna and for the mutual inductance $\Delta L_{12}(\omega)$ between the two antennae (*15*, *21*). The spatial periodicity of the microwave current density $j(x, \omega)$, as fixed by the meander shape of the antennae, determines the wave vector k of the excited spin waves. The Fourier transform $\tilde{j}(k, \omega)$ displayed in Fig. 1D shows a main peak at $k_M = 7.4\ \mu m^{-1}$ [that is, a wavelength (λ) ~ 0.8 μm corresponding to the spatial periodicity of the design] with a full width at half maximum (FWHM) of about 0.8 μm^{-1} alongside a secondary peak centered at $k_S = 2.8\ \mu m^{-1}$. In addition to the sample shown in Fig. 1, B and C, three other devices with different dimensions (w = 3.5 or 8 μm, λ ~ 0.8 or 1.6 μm, and D = 5.4 to 14.5 μm) were fabricated and studied.

We first characterized the permalloy strip and the propagation between the two antennae without dc current. Figure 2A shows the real and imaginary parts of the self-inductance ΔL_{11} for the w = 8 μm, λ ~ 1.6-μm sample under an applied field $\mu_0 H_0 = 0.993$ T. The absorption $Im(\Delta L_{11})$ displays two peaks: a main one at resonance frequency $f_{res} = 3.48$ GHz with a FWHM of 150 MHz and a secondary one at $f_{res} = 3.24$ GHz. They are attributed to the excitation of spin waves around k_M and k_S, respectively. The insets in Fig. 2A show the magnetic field dependency of the frequency of the main resonance (left) and the frequency dependence of its FWHM (right). These data are accounted fairly well by using the MSFVW dispersion (*15*) with a gyromagnetic ratio $\gamma/2\pi = 30.0$ GHz T^{-1}, an effective magnetization $\mu_0 M_{eff} = 0.88$ T, and a Gilbert damping factor $\alpha = 0.009$. These values compare reasonably well with the values obtained by broadband ferromagnetic resonance measurements on the unprocessed film (29.3 GHz T^{-1}, 0.94 T, and 0.006 T respectively) and with published values for permalloy/alumina thin films (*22*). Figure 2B shows the real and imaginary parts of the mutual inductance that were measured in the same run. One sees clear oscillations that are convoluted with the two absorption peaks observed in Fig. 2A. This is attributed to the propagation delay of the spin waves. When the frequency is swept around the f_{res}, slightly different wave vectors are selected within the FWHM of the $\tilde{j}(k,\omega)$ peaks so that the phase delay of the transmitted signal ($\phi = -kD$) changes continuously. From the period f_P of these oscillations, we estimate the spin wave group velocity to be $Vg = D\ f_P$ ~ 0.8 μm ns^{-1}, in reasonable agreement with the value of 0.72 μm ns^{-1} deduced from the MSFVW dispersion. The mutual inductances ΔL_{21} and ΔL_{12}, which correspond respectively to signal propagating in the forward (antenna 1→ 2) and reverse (antenna 2 → 1) directions, are identical (Fig. 2B), which confirms that the transmission of these volume spin waves is reciprocal (*19*, *20*) in the absence of a dc current.

Next, we proceeded to transmission measurements with a dc current. Figure 3A shows the imaginary part of the forward and reverse mutual inductances ΔL_{21} and ΔL_{12} measured for the w = 2 μm, λ ~ 0.8 μm sample upon injecting $I_{dc} = +6$ mA through the strip. The curves are shifted horizontally with respect to each other: The blue curve [$Im(\Delta L_{12})$], which corresponds to spin waves traveling in the same direction as the electron flow (Fig. 3A, inset), is shifted about 18 MHz higher in frequency than the red curve [$Im(\Delta L_{21})$], which accounts for spin waves traveling against the electron flow. When the polarity of the dc current is reversed (Fig. 3B), it is the red curve [$Im(\Delta L_{21})$], now corresponding to spin waves propagating along the electron flow, that is shifted about 18.5 MHz higher in frequency than the blue one. These observations were reproduced on all four samples, for different values of the dc current and for different values of the applied field (*15*). We also verified that the polarity of H_0 has no influence on the effect. To quantitatively compare these results, we plotted the measured frequency shifts Δf normalized by the wave vector k_M versus the electrical current density J (Fig. 3C). Aside from the data points corresponding to the highest current densities, we recognize a clear linear dependence in agreement with the STT Doppler shift. Upstream and downstream spin waves are Doppler-shifted in opposite ways so that the measured frequency shift Δf is two times the Δf_{STT} of Eq. 1. From the slope of the line shown in Fig. 3C, the spin polarization of the current in our permalloy film is estimated to be $P = 0.5 \pm 0.05$ (*15*), which indicates that the electrical current is mostly carried by the majority spins. The order of magnitude is consistent with the previous estimates derived from a detailed modeling of the low-temperature magnetoresistance of spin valves containing permalloy layers (P = 0.6 to 0.8) (*23*) and of the residual resistivity of bulk dilute alloys (P = 0.8 to 0.95) (*24*).

These results can be examined within the two-current model for which $P = \frac{\rho_\downarrow - \rho_\uparrow}{\rho_\downarrow + \rho_\uparrow}$, where the resistivities $\rho_\uparrow$ for the majority and $\rho_\downarrow$ for

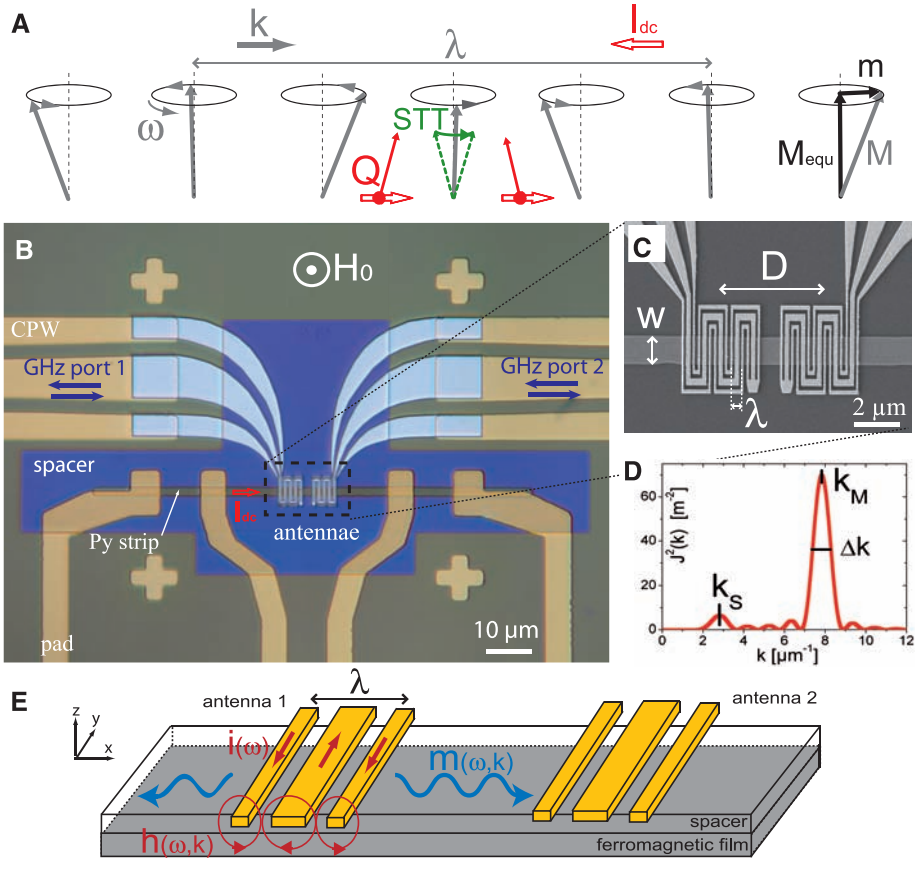

Fig. 1. Principle of the spin wave measurements. (**A**) Sketch of a spin wave subjected to STT [case of a spin wave propagating against the dc current (along the electron flow) with a spin polarization $P > 0$]. The red arrows represent the flow of spin-polarized electrons (the spin current Q) (*15*). (**B**) Optical micrograph of the device with a w = 2-μm permalloy strip (t = 20 nm) and a pair of λ = 0.8-μm antennae. (**C**) Scanning electron micrograph of the central region. (**D**) Fourier transform of the microwave current density for the antenna shown in (C). It was calculated by assuming a uniform current density across each branch of the meander. (**E**) Sketch of the operating principle of propagating spin wave spectroscopy.

the minority spin channels are determined by adding the contributions from the different sources of electron scattering (*24*). For bulk alloys at low temperature, the substitutional disorder dominates. Because the atomic potentials on Ni and Fe sites nearly align for the majority channel but differ substantially for the minority channel (*25*), this type of scattering is strongly spin-polarized in Ni-Fe ($\rho_{\downarrow} \sim 100$ microhm cm $>> \rho_{\uparrow}$) (*26*), which explains the very high value of P measured in these conditions (*24*). We estimate that several other sources of scattering contributed to the 30-microhm-cm room-temperature resistivity of our 20-nm polycrystalline film (to be compared with the residual resistivity 4 microhm cm of bulk permalloy): phonons and magnons (*24*), spin-mixing processes (*24*, *26*), grain boundaries, and film surfaces (*27*). This could explain the quantitative differences between our value of P and the previous estimates (*23*, *24*). Our experimental conditions were very close to those used to observe current-induced domain-wall motion (*7*, *8*, *28*), and so the polarization we measured is probably the most relevant in this context. The deviations from the linear dependence of $\Delta f/k$ versus J observed in Fig. 3C for current densities $|J| > 1.2\ 10^{11}$ A m^{-2} could reflect the enhancement of magnon and phonon scattering (*24*) due to a sizable Joule heating ($\Delta T \sim 100$ K for the $w = 3.5$-μm sample under $|J| = 1.7\ 10^{11}$ A m^{-2}, as estimated from the changes of the strip resistance and resonance frequency) (*15*). In line with these observations, a systematic study of the dependence of the Doppler shift on temperature, film thickness, and material microstructure could help to elucidate the scattering mechanisms that govern the adiabatic spin transfer in various materials. Spin waves could also be used to test the existence of the controversial nonadiabatic term of STT (*8*, *12*–*14*). Such a term would result in a simple change of the propagating attenuation of the spin waves, which could be accessed by improving the am-

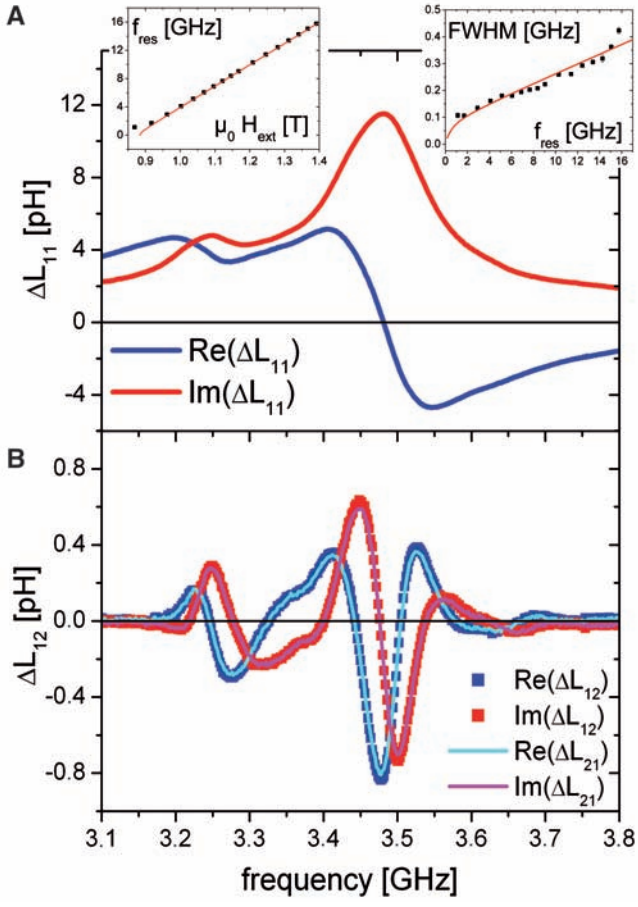

Fig. 2. Characterization of the spin wave signals in the absence of dc current. (**A**) Self-inductance measurement for a $\lambda = 1.6$-μm antenna coupled to a $t = 20$-nm, $w = 8$-μm permalloy strip subjected to a $\mu_0 H_0 = 0.993$ T field. (Left) Magnetic field dependence of the main resonance frequency. The continuous line was calculated with the dispersion of MSFVW (SOM text) (*15*). (Right) Frequency dependence of the frequency-swept linewidth (FWHM) of the main resonance. The continuous line was calculated by adding the intrinsic Gilbert contribution (*15*) to the inhomogeneous broadening because of the finite wave vector spreading of the excitation (Fig. 1D). (**B**) Mutual inductance measurements for the same experimental conditions ($D = 8.7$ μm).

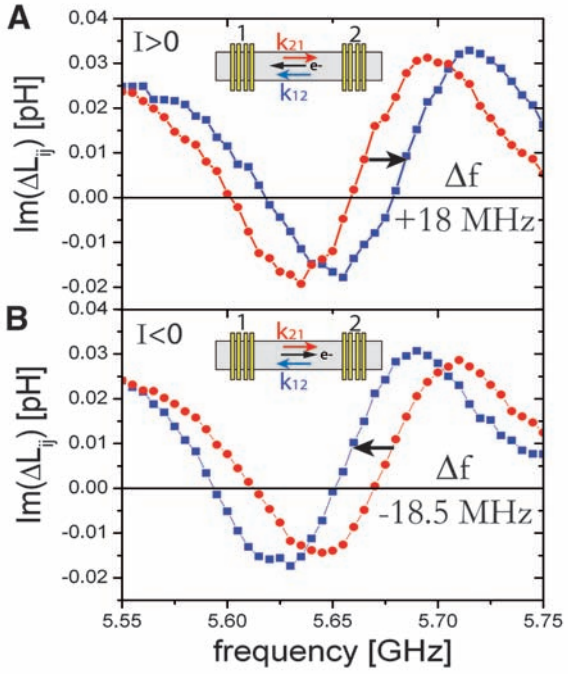

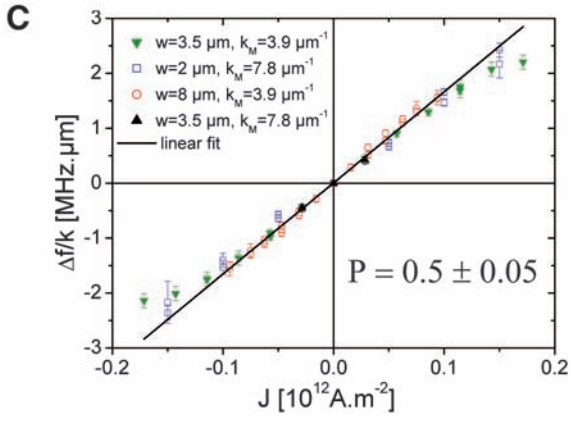

Fig. 3. Influence of a dc current on the spin wave propagation. (**A**) Mutual-inductance measurement in the presence of a $I = +6$ mA dc current for the $w = 2$ μm, $\lambda = 0.8$ μm sample under $\mu_0 H_0 = 1.029$ T. ΔL_{21} is shown as a red curve and corresponds to spin waves propagating from antenna 1 to antenna 2. ΔL_{12} is shown as a blue curve and corresponds to spin waves propagating from antenna 2 to antenna 1. The orientations of the spin wave wave vector and of the electron flow are shown in the inset. The measured frequency shift Δf is indicated on the graph. For clarity, only the imaginary part and only the frequency range corresponding to the main peak ($k \approx k_M$) are shown. (**B**) I_{dem} for $I = -6$ mA. (**C**) Experimental k-normalized frequency shifts versus current density. The data has been collected on four different devices and, in most cases, for two different magnetic fields (so that the main resonance falls in the ranges of 3 to 4 GHz and 4 to 7 GHz). The linear fit was performed in the range $|J| < 1.2\ 10^{11}$ A m^{-2}. P was determined with Eq. 1 and a product $M_s t$, which was deduced from the resonance data (*15*).

plitude stability of the PSWS experiment. Such studies could help to promote a fundamental understanding of spin-polarized transport in various itinerant ferromagnets, in that spin waves provide both a well-defined inhomogeneous magnetization configuration for performing spin transfer and an accurate probe with which to measure it.

References and Notes

1. J. C. Slonczewski, *J. Magn. Magn. Mater.* **159**, L1 (1996).
2. L. Berger, *Phys. Rev. B* **54**, 9353 (1996).
3. E. B. Myers, D. C. Ralph, J. A. Katine, R. N. Louie, R. A. Buhrman, *Science* **285**, 867 (1999).
4. M. D. Stiles, J. Miltat, in *Spin Dynamics in Confined Magnetic Structures* (Springer, New York, 2006), vol. 3, pp. 225–308.
5. M. Tsoi *et al.*, *Nature* **406**, 46 (2000).
6. W. H. Rippard, M. R. Pufall, in *Handbook of Magnetism and Advanced Magnetic Materials*, H. Kronmüller, S. Parkin, Eds (Wiley, New York, 2007), vol. 2, pp. 1167–1191.
7. A. Yamaguchi *et al.*, *Phys. Rev. Lett.* **92**, 077205 (2004).
8. L. Thomas, S. Parkin, in *Handbook of Magnetism and Advanced Magnetic Materials*, H. Kronmüller, S. Parkin, Eds (Wiley, New York, 2007), vol. 2, pp. 942–982.
9. Y. B. Bazaliy, B. A. Jones, S. C. Zhang, *Phys. Rev. B* **57**, R3213 (1998).
10. J. Fernández-Rossier, M. Braun, A. S. Nuñez, A. H. MacDonald, *Phys. Rev. B* **69**, 174412 (2004).
11. L. L. Hirst, *Phys. Rev.* **141**, 503 (1966).
12. S. Zhang, Z. Li, *Phys. Rev. Lett.* **93**, 127204 (2004).
13. A. Thiaville, Y. Nakatani, J. Miltat, Y. Suzuki, *Europhys. Lett.* **69**, 990 (2005).
14. J. Xiao, A. Zangwill, M. D. Stiles, *Phys. Rev. B* **73**, 054428 (2006).
15. Materials and Methods are available as supporting material on *Science* Online.
16. T. P. Gill, *The Doppler Effect, An Introduction to the Theory of the Effect* (Logos Press, London, 1965).
17. D. D. Stancil, B. E. Henty, A. G. Cepni, J. P. Van't Hof, *Phys. Rev. B* **74**, 060404 (2006).
18. P. Lederer, D. L. Mills, *Phys. Rev.* **148**, 542 (1966).
19. A. G. Gurevich, G. A. Melkov, *Magnetization Oscillations and Waves* (CRC Press, 1996).
20. D. D. Stancil, *Theory of Magnetostatic Waves* (Springer, New York, 1993).
21. M. Bailleul, D. Olligs, C. Fermon, *Appl. Phys. Lett.* **83**, 972 (2003).
22. H. Hurdequint, *J. Magn. Magn. Mater.* **242–245**, 521 (2002).
23. J. Bass, W. P. Pratt Jr., *J. Magn. Magn. Mater.* **200**, 274 (1999).
24. I. A. Campbell, A. Fert, in *Ferromagnetic Materials*, E. P. Wohlfarth, Ed. (North-Holland, Amsterdam, 1982), vol. 3, pp. 747–804.
25. P. E. Mijnarends, S. Sahrakorpi, M. Lindroos, A. Bansil, *Phys. Rev. B* **65**, 075106 (2002).
26. J. Banhart, H. Ebert, A. Vernes, *Phys. Rev. B* **56**, 10165 (1997).
27. A. F. Mayadas, J. F. Janak, A. Gangulee., *J. Appl. Phys.* **45**, 2780 (1974).
28. G. S. D. Beach, C. Knutson, C. Nistor, M. Tsoi, J. L. Erskine, *Phys. Rev. Lett.* **97**, 057203 (2006).

29. We thank J. Grollier and C. Deranlot (UMR CNRS/Thalès) for providing the permalloy films, H. Hurdequint for advice, A. Carvalho for assistance with e-beam lithography, A. Boulard for the fabrication of the measurement set-up, and K. Hajjia for measurements on unprocessed films. Support from the staff of the Consortium de Nanosciences et de Nanotechnologies de Strasbourg nanofabrication facilities and financial support from Agence Nationale de la Recherche "spectrospin" and from Region Alsace are gratefully acknowledged.

Supporting Online Material

www.sciencemag.org/cgi/content/full/322/5900/410/DC1
Materials and Methods
SOM Text
Figs. S1 and S2
References

7 July 2008; accepted 10 September 2008
10.1126/science.1162843

Complex Patterning by Vertical Interchange Atom Manipulation Using Atomic Force Microscopy

Yoshiaki Sugimoto,[1] Pablo Pou,[2] Oscar Custance,[3]* Pavel Jelinek,[4] Masayuki Abe,[1,5] Ruben Perez,[2] Seizo Morita[1]

The ability to incorporate individual atoms in a surface following predetermined arrangements may bring future atom-based technological enterprises closer to reality. Here, we report the assembling of complex atomic patterns at room temperature by the vertical interchange of atoms between the tip apex of an atomic force microscope and a semiconductor surface. At variance with previous methods, these manipulations were produced by exploring the repulsive part of the short-range chemical interaction between the closest tip-surface atoms. By using first-principles calculations, we clarified the basic mechanisms behind the vertical interchange of atoms, characterizing the key atomistic processes involved and estimating the magnitude of the energy barriers between the relevant atomic configurations that leads to these manipulations.

Scanning tunneling microscopy (STM) has proven to be the method of excellence for creating nanostructures on surfaces, manipulating atoms and molecules one at a time (*1*–*3*). A new panorama has recently been opened by the capability of atomic force microscopy (AFM) to create similar nanostructures atom by atom (*4*) and to quantify the forces involved in these lateral manipulations (*5*, *6*).

When exploring a surface with these scanning probe methods, the apex of the probe can be contaminated with atomic species present at the surface (*7*) by picking up atoms in accidental or intended mechanical contacts with the surface. Advantage could be taken of this situation, and an atomic version of the dip-pen nanolithography (*8*) may be implemented: Atoms wetting the tip apex could be individually deposited to write patterns at heterogeneous surfaces. We provide evidence that such an atomic pen can be implemented by using AFM.

We performed the AFM experiments (*9*) in dynamic mode under the frequency modulation detection scheme (*10*), keeping the cantilever oscillation amplitude constant. Commercial silicon cantilevers, which have very sharp tips at their free ends, were used to image the Sn/Si(111) – $(\sqrt{3} \times \sqrt{3})$R30° surface (*11*) by detecting the short-range chemical interaction force between the closest tip and surface atoms (*9*).

The inset of Fig. 1A shows topographic images of a single atomic layer of tin (Sn) atoms, which appear as bright protrusions, grown over a silicon (111) single-crystal substrate. Among the atomic defects this surface exhibits (*11*), the most representative ones are substitutional silicon (Si) atoms (*12*) at the perfect Sn atomic layer, and these appear as protrusions with diminished contrast. We have observed that these Si defects can be vertically manipulated during force spectroscopy (*13*, *14*) experiments. After imaging the surface and positioning the AFM tip with a lateral precision better than ±0.1 Å (*15*) over the topmost part of the marked Si atom, we moved the sample toward the oscillating AFM probe. At a given tip-surface distance, an instability in the frequency shift occurs, as highlighted by the arrow in the graph. In an image taken after the sample was retracted, the Si atom was no longer visible, and a Sn atom was found to occupy the corresponding lattice position instead (Fig. 1A, bottom right inset). One hypothesis to explain this event is that the Si atom at the surface has been replaced by a Sn atom originally located at the tip apex, as sketched out by the illustration in Fig. 1A. The same procedure can be consecutively applied to the freshly deposited Sn atom (marked with a circle in Fig. 1B, left inset), resulting in the replacement of this surface atom by a Si atom coming from the tip and in a partial loss of atomic contrast (Fig. 1B, bottom right inset). Because all the images shown in Fig. 1 were acquired under the same experimental parameters,

[1]Graduate School of Engineering, Osaka University, 2-1 Yamada-Oka, 565-0871 Suita, Osaka, Japan. [2]Departamento de Física Teórica de la Materia Condensada, Universidad Autónoma de Madrid, 28049 Madrid, Spain. [3]National Institute for Materials Science, 1-2-1 Sengen, 305-0047 Tsukuba, Ibaraki, Japan. [4]Institute of Physics, Academy of Sciences of the Czech Republic, Cukrovarnicka 10, 1862 53 Prague, Czech Republic. [5]Precursory Research for Embryonic Science and Technology, Japan Science and Technology Agency (JST), 332-0012 Saitama, Japan.

*To whom correspondence should be addressed. E-mail: custance.oscar@nims.go.jp